American Mineralogist, Volume 83, pages 248–258, 1998

Replacement of primary monazite by apatite-allanite-epidote coronas in an amphibolite facies granite gneiss from the eastern Alps

Fritz Finger, Igor Broska,* Malcolm P. Roberts, and Andreas Schermaier

Institut für Mineralogie der Universität Salzburg, Hellbrunnerstrasse 34, A-5020 Salzburg, Austria

Abstract

Accessory monazite crystals in granites are commonly unstable during amphibolite facies regional metamorphism and typically become mantled by newly formed apatite-allanite-epidote coronas. This distinct textural feature of altered monazite and its growth mechanism were studied in detail using backscattered electron imaging in a sample of metagranite from the Tauern Window in the eastern Alps. It appears that the outer rims of the former monazites were replaced directly by an apatite ring with tiny thorite intergrowths in connection with Ca supply through metamorphic fluid. Around the apatite zone, a proximal allanite ring and a distal epidote ring developed. This concentric corona structure, with the monazite core regularly preserved in the center, shows that the reaction kinetics were diffusion controlled and relatively slow.

Quantitative electron microprobe analyses suggest that the elements released from monazite breakdown (P, REE, Y, Th, U), were diluted and redistributed in the newly formed apatite, allanite, and epidote overgrowth rings and were unable to leave the corona. This supports the common hypothesis that these trace elements are highly immobile during metamorphism. Furthermore, microprobe data suggest that the preserved monazite cores lost little, possibly none of their radiogenic lead during metamorphism. Thus, metastable monazite grains from orthogneisses appear to be very useful for constraining U-Th-Pb protolith ages.

On the basis of these findings and a review of literature data, it seems that monazite stability in amphibolite facies metamorphic rocks depends strongly on lithologic composition. While breaking down in granitoids, monazite may grow during prograde metamorphism in other rocks such as metapelites.

Introduction

The LREE-phosphate monazite is widely reported as an accessory mineral in peraluminous granitoids and high-grade metamorphic gneisses. Despite its very minor occurrence and generally small size, monazite is nevertheless of outstanding geological importance. First, it is very useful for geochronology, because it incorporates large quantities of Th and U (Parrish 1990; Montel et al. 1996). Second, monazite crystals typically carry between 40 and 80% of the LREE content of their host rock (Bea 1996; Schitter 1997). Thus, monazite growth, fractionation, or destruction in the course of various geological processes has the potential to influence greatly the REE systematics of rocks. Considering this, it is surprising that the stability relations of monazite have attracted relatively little interest. Although important data are available on monazite solubility in felsic melts (Rapp and Watson 1986; Montel 1993). However, very little is known about monazite-forming or -destroying reactions during metamorphism. For example, it is commonly believed that monazite is stable under medium- to high-grade metamorphic conditions, but that monazite often reacts to allanite or apatite over the temperature range of low-grade conditions (Overstreet 1967; Bons 1988; Ward et al. 1991; Smith and Barreiro 1990; Lanzirotti and Hanson 1996). In this paper, we document the partial replacement of accessory magmatic monazite by an apatite-allanite-epidote paragenesis, which formed when the host peraluminous granite was metamorphosed under amphibolite facies conditions. Using quantitative electron microprobe analysis, we discuss the element redistribution that occurred in conjunction with monazite breakdown. Lastly, we discuss some potential implications of our findings for U-Th-Pb geochronology using monazite.

Investigated rock

The monazite replacement process was investigated using a sample of S-type granite gneiss from the central eastern Alps (Granatspitz massif, Tauern Window Fig. 1). The magmatic formation age of the rock is about 320–330 Ma (Cliff 1981). Amphibolite facies metamorphism in the Tauern Window occurred during the Tertiary in connection with Alpine orogenesis. The exposed rocks

* Present address: Geological Institute of the Slovak Academy of Sciences, Dubravska Cesta 9, 842 26 Bratislava, Slovakia.

0003–004X/98/0304–0248$05.00

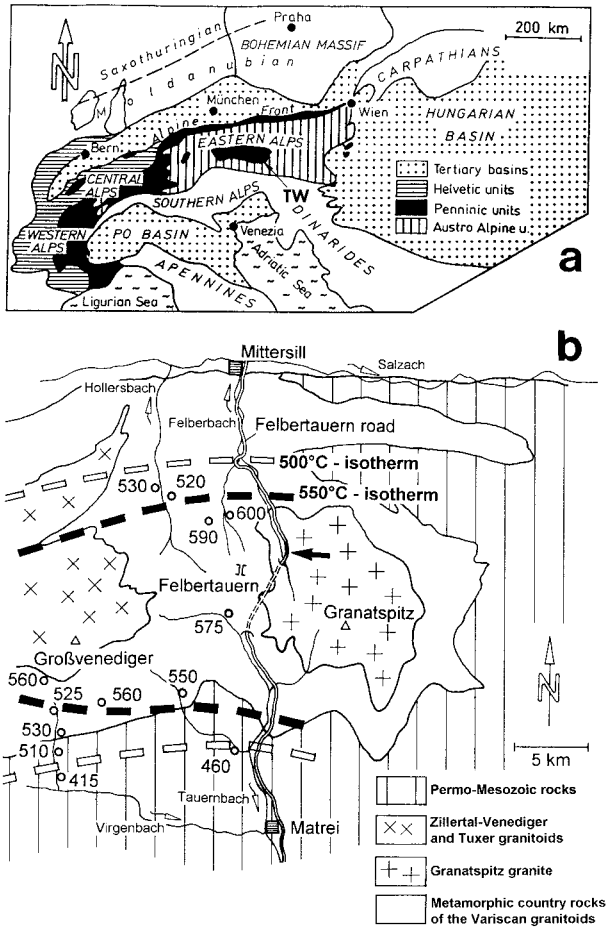

FIGURE 1. Sample location and geological setting. (**a**) Position of the Tauern Window (TW) within the geological framework of central Europe. This tectonic window exposes the Penninic unit, which is the lowermost structural zone of the eastern Alps. For more detailed geological information see Frasl (1958) and Frank et al. (1987). (**b**) Geological sketch map of the central Tauern Window. The Granatspitz granite massif is one of the numerous metamorphosed Variscan plutons that occur as domes along the central axis of the Tauern Window (Finger et al. 1993). The sample chosen for this study (arrow) was collected near the Felbertauern mountain road, at the Ödalm, where several fresh boulders of typical Granatspitz granite gneiss had been brought down by a local landslide. The degree of Alpine metamorphism reached about 550–600 °C and 5–6 kbar in this area (Frank et al. 1987). The temperatures and metamorphic isograds shown are taken from Hoernes and Friedrichsen (1974) and based on O isotope thermometry.

form an E-W-oriented thermal and tectonic dome structure (Fig. 1). Pressure-temperature conditions of the Alpine-age metamorphism in the Tauern Window range from about 4–5 kbar and 400–500 °C at its periphery to about 6 kbar and 600 °C in the center (Dachs 1986; Frank et al. 1987).

The sample used for this study is highly representative of the Granatspitz massif. It is a little deformed, medium- to coarse-grained two-mica gneiss with some green biotite-muscovite pseudomorphs after cordierite (Frasl 1967). Magmatic textures are widely preserved in the rock. Alpine metamorphism caused a slight filling of the plagioclases with white mica and some epidote or clinozoisite grains, exsolution of rutile (sagenite) and ilmenite in biotite, partial alteration of biotite to muscovite, and recrystallization of small quartz crystals and some oligoclase along grain boundaries. There is no textural or mineralogical evidence for any later major low-*T* overprinting. The chemical and modal composition of the rock is given in Table 1.

TABLE 1. Chemical and modal composition of the Granatspitz gneiss

wt% oxides		Trace elements (ppm)		Rare earth elements (ppm)		Modal mineralogy	
SiO_2	70.91	Cr	7	La	24.1	Qtz	31
TiO_2	0.24	Rb	249	Ce	50.8	Kfs	31
Al_2O_3	14.83	Sr	81	Nd	22.3	Pl	28
FeO*	1.65	Y	11	Sm	5.05	Bt	5
MnO	0.03	Zr	93	Eu	0.58	Ms	3
MgO	0.42	Nb	5	Tb	0.67	Acc	2
CaO	1.28	Ba	339	Yb	1.48		
Na_2O	3.01	Th	16	Lu	0.21		
K_2O	5.09						
P_2O_5	0.23						
L.O.I.	0.84						
Total	98.53						

Note: FeO* = total iron as FeO. Mineral abbreviations after Kretz (1983) except Acc = accessory minerals.

MICROTEXTURES OF MONAZITE REPLACEMENT

The transformation of the accessory monazite grains to apatite, allanite, and epidote can be best studied in backscattered electron (BSE) images (Fig. 2). The crystals are mostly 20 to 50 μm in size, rarely up to 100 μm. The transformed grains are always characterized by a distinct corona structure, with a preserved monazite core in the center and a mantle of apatite, allanite, and epidote as concentric growth rings.

The *monazite zone* in the center of the pseudomorphs generally appears fairly homogeneous in the BSE image. In some cases, faint concentric compositional zonation may be seen, which is interpreted as a magmatic growth feature (see next section).

The *apatite zone* surrounds the monazite zone and is rarely more than a few micrometers wide. In most cases it appears spotty in the BSE image (Fig. 2). This spotty texture results mainly from the intergrowth of many small thorite crystals, which produce bright spots in the BSE image. In a few cases, tiny monazite islands were identified within the apatite zone. These seem to testify that the apatite is directly replacing primary monazite. Also, because apatite formed adjacent to only the preserved monazite core, it appears that the phosphorous required for apatite growth came directly from the breakdown of monazite. The outer rim of the apatite zone is mostly euhedral to subhedral (Fig. 2), which suggests that it may represent the former rim of the primary monazite grain.

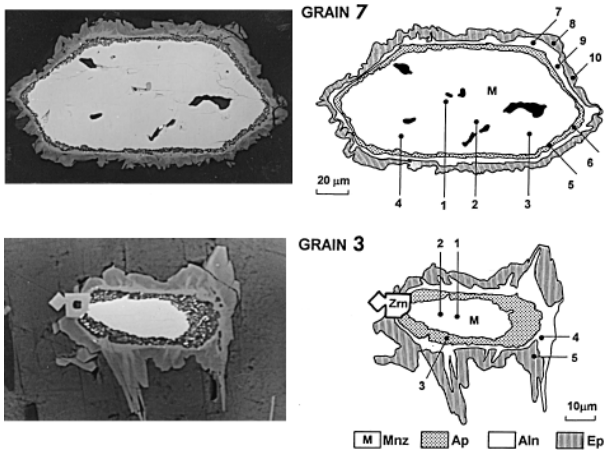

FIGURE 2. Representative BSE-images of partially replaced relatively large, accessory monazites from the Granatspitz granite gneiss. The sketches beside each photograph are schematic illustrations of the different mineral zones. Grain 3 has grown contemporaneously with two small magmatic zircon crystals and is hosted by biotite (note the cleavage). Grain 7 is a single crystal obtained from a heavy mineral fraction and is embedded in epoxy resin. Numerals refer to microprobe point analyses listed in Table 2. Mineral abbreviations are those recommended by Kretz (1983).

These observations indicate that apatite was only able to grow within or at least very close to the former monazite lattice.

The *allanite zone* mantles the apatite zone and always appears relatively bright in the BSE images (Fig. 2). In general, it has roughly the same width as the apatite zone. However the outer boundaries of the allanite zone are typically anhedral, with spiky and lobate protrusions into the epidote mantle. Thus, it appears that the allanite zone is not strictly replacing earlier monazite, but developing largely outside of the former monazite grain after the latter had been partially replaced by apatite.

The *epidote zone* always forms the outer shell of the corona. It is typically more voluminous than the allanite zone. The epidote apparently invades the minerals that host the former monazite grains preferentially along their cleavage planes (Fig. 2, grain 3).

The extent to which monazite is replaced differs from grain to grain. In some cases, it appears that more than 50 vol% of the original monazite fell victim to the transformation process. In other grains, the reaction products form only a thin rim, where not more than 10 vol% of the monazite was altered. Within some larger apatite crystals, armored monazite inclusions occur that lack evidence of transformation. The strongest alteration commonly is found in monazites located along grain boundaries of the major rock-forming minerals or along cleavage planes of biotite and plagioclase. This pattern suggests that the CaO, SiO_2, Al_2O_3, and FeO required for apatite-allanite-epidote corona formation were supplied by a fluid phase.

In general, it appears that where the apatite zone is small then the allanite and the epidote zones are also small, and vice versa. These observations indicate some kind of stoichiometric control on the replacement reaction and clearly argues against a purely metasomatic process. The almost perfectly concentric arrangement of apatite, allanite, and epidote growth zones implies that the transformation process was governed primarily by the kinetics of the outward diffusion of elements derived from the monazite. This is discussed later in more detail.

ANALYTICAL RESULTS

The monazite zone

Eight relict monazite grains were analyzed. All had fairly similar compositions. Examples of analyses from the two grains shown in Figure 2 are given in Table 2 together with their mineral formulae calculated on the basis of four O atoms. The monazite compositions are a solid solution consisting dominantly of the LREE-phosphate end-member (monazite s.s.), with about 5–10% each of the huttonite ($ThSiO_4$), brabantite [$CaTh(PO_4)_2$] and xenotime (Y-HREE-PO_4) components.

Generally, the highest La contents and La/Sm ratios were measured in the center of the monazite grains. Both values tend to decrease slightly with distance from the center of the grain. Conversely, Y contents increase outward (Figs. 2 and 3). This kind of chemical zonation most likely reflects normal magmatic crystal/liquid fractionation involving early monazite crystallization with successively greater depletion of the melt in those elements with the highest monazite/melt K_D values (Wark and Miller 1993). Also, the huttonite/brabantite ratio may be higher in the centers of the monazites; this is a commonly observed feature in magmatic monazites (I. Broska, unpublished results).

The theoretical REE pattern for magmatic monazite has been calculated from the whole-rock data (Table 1) using the K_D values from Cocherie (1984) and Sawka (1988) and the simple relation $C_{Mon} = C_{WR}*K_D$. The calculated pattern is similar to the monazite core composition (Fig. 3), suggesting that monazite crystallized early in chemical equilibrium with granite melt.

The apatite zone

In most microprobe analyses carried out in the apatite zone, significant amounts of ThO_2 were recorded (Table 2), including domains that appear to be free of any bright thorite spots in the BSE image. Only in a few analyzed points could a Th-poor apatite composition be obtained (e.g., Table 2, analysis 6). Likewise, pure thorite compositions could be obtained only in a very few of the bigger bright spots. Therefore, it seems that apatite and thorite are intergrown on an extremely fine scale, which is beyond the spatial resolution of the microprobe.

On the basis of measurements obtained with an expanded 5 µm diameter beam, we integrated the average composition of the thorite plus apatite mixture that forms the apatite zone. The mean composition of this mixture

TABLE 2. Microprobe analyses and mineral formulae from the grains illustrated in Figure 2

	Grain 7										Grain 3				
	1 mon	2 mon	3 mon	4 mon	5 ap	6 ap	7 all	8 all	9 ep	10 ep	1 mon	2 mon	3 ap	4 all	5 ep
P_2O_5	27.76	27.71	28.28	28.65	37.02	39.26	n.d.	n.d.	n.d.	n.d.	28.53	29.56	37.11	n.d.	n.d.
SiO_2	0.69	0.87	0.41	0.47	1.95	1.31	32.16	31.72	35.48	35.77	0.72	0.57	2.53	32.20	35.08
La_2O_3	13.05	13.33	13.51	12.88	0.89	0.75	5.57	6.05	2.22	2.21	11.69	10.55	0.48	5.77	2.69
Ce_2O_3	27.53	28.57	29.00	25.56	1.58	1.15	11.25	12.68	5.62	5.90	26.78	25.26	0.91	11.34	6.52
Pr_2O_3	3.29	3.21	3.58	3.81	0.10	0.12	1.52	1.60	0.85	0.85	3.77	3.60	0.10	1.41	0.72
Nd_2O_3	11.36	11.12	11.54	11.93	0.88	0.54	4.50	3.96	2.75	2.87	12.89	12.55	0.40	3.73	3.12
Sm_2O_3	1.81	1.70	2.09	2.35	0.23	0.10	0.73	0.32	0.93	0.74	2.03	2.55	0.01	0.75	0.53
Y_2O_3	0.97	0.99	2.01	2.67	0.24	0.16	0.16	0.05	1.05	1.12	1.69	2.98	0.15	0.25	0.93
ThO_2	9.01	9.29	7.78	8.84	3.92	0.63	1.05	1.36	0.21	0.22	8.70	9.29	6.85	1.35	0.18
UO_2	0.24	0.36	0.36	0.59	0.03	0.03	0.07	0.05	0.28	0.31	0.20	0.34	0.12	0.03	0.23
Al_2O_3	n.d.	n.d.	n.d.	n.d.	n.d.	n.d.	18.33	17.19	22.34	24.38	n.d.	n.d.	n.d.	19.38	23.95
FeO	n.d.	n.d.	n.d.	n.d.	n.d.	n.d.	10.82	10.92	7.85	7.77	n.d.	n.d.	n.d.	9.19	8.17
CaO	1.31	1.10	1.18	1.49	50.17	52.29	11.79	10.75	16.74	15.83	1.10	1.47	48.99	11.28	15.55
MgO	n.d.	n.d.	n.d.	n.d.	n.d.	n.d.	0.30	0.32	0.26	0.28	n.d.	n.d.	n.d.	0.30	0.27
F	n.d.	n.d.	n.d.	n.d.	3.06	3.01	n.d.	n.d.	n.d.	n.d.	n.d.	n.d.	3.10	n.d.	n.d.
Total	97.04	98.24	99.74	99.24	100.06	99.36	98.27	96.98	96.55	98.24	98.10	98.70	100.74	96.97	97.93
O = F	0.00	0.00	0.00	0.00	1.29	1.27	0.00	0.00	0.00	0.00	0.00	0.00	1.31	0.00	0.00
Total	97.04	98.24	99.74	99.24	98.77	98.09	98.27	96.98	96.55	98.24	98.10	98.70	99.44	96.97	97.93
P	0.962	0.954	0.959	0.966	5.626	5.824	n.d.	n.d.	n.d.	n.d.	0.971	0.984	5.621	n.d.	n.d.
Si	0.028	0.036	0.016	0.019	0.350	0.230	2.959	2.993	3.024	2.986	0.029	0.022	0.453	2.968	2.962
La	0.197	0.200	0.200	0.189	0.059	0.049	0.189	0.210	0.070	0.068	0.173	0.153	0.031	0.196	0.084
Ce	0.413	0.425	0.426	0.373	0.104	0.074	0.379	0.438	0.175	0.180	0.394	0.364	0.060	0.383	0.201
Pr	0.049	0.047	0.052	0.055	0.007	0.008	0.051	0.055	0.026	0.026	0.055	0.052	0.007	0.047	0.022
Nd	0.166	0.161	0.165	0.170	0.057	0.034	0.148	0.134	0.084	0.086	0.185	0.176	0.026	0.123	0.094
Sm	0.026	0.024	0.029	0.032	0.014	0.006	0.023	0.011	0.027	0.021	0.028	0.035	0.001	0.024	0.015
Y	0.021	0.021	0.043	0.057	0.023	0.015	0.008	0.002	0.048	0.050	0.036	0.062	0.014	0.012	0.042
Th	0.084	0.086	0.071	0.084	0.160	0.025	0.022	0.029	0.004	0.004	0.080	0.083	0.279	0.028	0.003
U	0.002	0.003	0.002	0.005	0.001	0.001	0.000	0.000	0.005	0.006	0.002	0.003	0.005	0.001	0.004
Al	n.d.	n.d.	n.d.	n.d.	n.d.	n.d.	1.987	1.912	2.244	2.398	n.d.	n.d.	n.d.	2.105	2.383
Fe	n.d.	n.d.	n.d.	n.d.	n.d.	n.d.	0.832	0.861	0.559	0.542	n.d.	n.d.	n.d.	0.708	0.576
Ca	0.058	0.048	0.051	0.064	9.649	9.816	1.162	1.086	1.528	1.416	0.047	0.062	9.391	1.114	1.407
Mg	n.d.	n.d.	n.d.	n.d.	n.d.	n.d.	0.041	0.044	0.033	0.034	n.d.	n.d.	n.d.	0.041	0.034
F	n.d.	n.d.	n.d.	n.d.	1.735	1.669	n.d.	n.d.	n.d.	n.d.	n.d.	n.d.	1.754	n.d.	n.d.

Note: Formula proportions of cations based on 4 O atoms (monazite); 3 O atoms (apatite), and 12.5 O atoms (allanite and epidote). Numbers in the second row refer to analysis points shown in Figure 2. n.d. = not detected.

(Table 3) is broadly similar in all measured grains, and it shows that the estimated proportion of thorite in the apatite zone is approximately 7 wt%.

It appears from the analytical results that the apatite lattice contains a relatively high amount of the lessingite component $[Ca_2(REE)_3(SiO_4)_3(F,OH)]$ (see analysis 6 in Table 2). Because the apatite zone is generally very narrow, we cannot preclude the possibility that the measured concentrations of REE and Y are enhanced by X-rays excited from neighboring monazite or allanite zones. However, we consider this potential contamination effect to be minor because first, when non-stoichiometric analyses were excluded the concentrations of REE and Y are roughly the same in narrower and broader sectors of the apatite zones. Second, no Al or Fe was detected in the stoichiometric apatite analyses, which suggests that no allanite was involved. Third, REE in the apatite appear to be broadly balanced by Si, following correction for thorite content, which would not be the case if the REE were derived from monazite excitation.

The chondrite-normalized LREE patterns of the apatite zone and the monazite zone are subparallel, but the La/Y ratios are significantly lower in the apatite zone (Fig. 3). Nevertheless, the La/Y ratios are still fairly high for apatite. As an example, Figure 3 shows a hypothetical magmatic apatite pattern calculated with literature K_D values (Sawka et al. 1988) from the whole-rock composition of the sample. This pattern lies at much lower levels and its shape is clearly flatter, which suggests that the apatite zone inherited its enriched and steeply fractionated pattern from the pre-existing monazite. For comparison, some of the normal accessory apatites of the sample were analyzed. Their LREE contents were always close to the detection limit (Ce_2O_3 is about 0.05–0.1%), which is roughly 5 to 10 times lower than the REE content recorded in the apatite coronas (as predicted by the K_D modeling).

The allanite zone

REE+Y+Th make up between 0.8–1 atoms per formula unit (apfu) in the allanite zone, indicating that only a small amount of clinozoisite-epidote solid-solution component is present (Table 2). The Al contents are high compared to normal magmatic allanite from granitoids (Petrik et al. 1995), which implies that not much ferriallanite component is present. Generally the allanite zone has the same compositional range in all analyzed grains. However, microprobe profiles show that slight compositional zoning exists across the allanite rings in most cases (Fig. 4), with decreasing LREE (La-Nd) and increasing

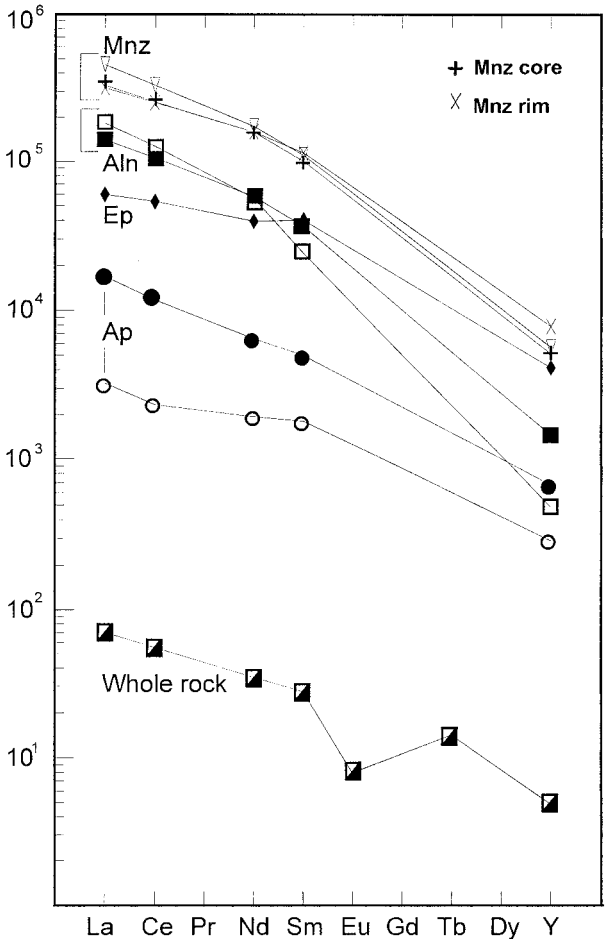

FIGURE 3. Chondrite-normalized REE variation diagram for selected light and middle REE, showing the REE chemistry of the whole-rock, the monazite and the minerals in the alteration coronas using the averages from Table 3. Heavy REE were not determined due to very low concentrations below or near to the detection limit. However, it can be assumed that their behavior approximates that of Y (included on the diagram in the place of Ho). Normalization values used are those of Wakita et al. (1971). Filled symbols and crosses are measured concentrations. Open symbols are theoretical equilibrium compositions of magmatic monazite, apatite, and allanite calculated from the whole-rock composition using the K_D values of Cocherie (1984) and Sawka (1988) and the expression $C_{calc} = C_{WR} * K_D$.

Y and U outward. The REE variation is apparently balanced mainly by the substitution: $LREE^{3+}(A2) + Fe^{2+}(M1) = Ca^{2+}(A2) + Al^{3+}(M1)$ (Dollase 1971).

La/Nd, Nd/Sm, and LREE/Y ratios in the allanite zone are on average somewhat higher than in the monazite zone. The chondrite-normalized REE pattern of the allanite zone is thus steeper than that of the monazite (Fig. 3), but flatter than that of magmatic allanites from granitoids (see data compilation in Petrik et al. 1995). Using published K_D values (Cocherie 1984) and the whole-rock composition of the sample, we estimate that early magmatic allanite in equilibrium with the granitic magma would have a much steeper LREE pattern (Fig. 3).

The epidote zone

Analyses from the epidote zone reveal little grain to grain compositional variation. Approximately 0.35–0.5 REE apfu substitute for Ca in the A2 position. This means that the epidote zone contains a considerable allanite solid-solution component. Nevertheless, a clear compositional gap separates the epidote zone from the allanite zone (Fig. 4). This compositional gap, which may reflect some kind of solvus behavior, is clearly seen in the BSE images.

The Al content of the epidote zone is between 2.1 and 2.4 apfu, indicating the presence of a clinozoisite component. From the REE+Y+Th content, which is around 0.5 apfu, it appears that only about 50 wt% of the total Fe in the epidote zone occurs as Fe^{3+} (Petrik et al. 1995).

Like the allanite zone, slight compositional zoning occurs across the epidote zone in most cases, in which the La and Ce contents decrease outward (Fig. 4). This systematic decrease in La and Ce is compensated for by increasing Ca in the A2 position accompanied by increasing Al and decreasing Fe. Thus, the overall effect is an increasing clinozoisite component rimward. Neodymium, Sm, Y, and U show the reverse behavior compared with La and Ce and display a slight increase outward across the epidote zone (Fig. 4). Figure 3 shows that the LREE-Y distribution in the epidote zone is much flatter than in the allanite zone. Lanthanum contents in the epidote zone are approximately half of those in the allanite zone. However the amount of Sm in the epidote is higher than in the allanite. Yttrium contents are about three times higher in the epidote zone than in the allanite zone and reach values almost equivalent to the monazite. Th is relatively low in the epidote zone, whereas UO_2 (0.2–0.4 wt%) is fairly high.

DISCUSSION

The chemical budget of the alteration reaction

High field-strength trace elements, such as those required for the formation of monazite (P, LREE, Y, Th) are commonly considered to be highly immobile during metamorphism. Thus it was interesting to determine whether, from the chemical point of view, the new coronas around the monazites may be viewed simply as a ''diluted'' monazite, fed with additional Ca, Fe, Al, and Si. To test this hypothesis, a model calculation was carried out. In a first step, the mean modal composition of the corona systems was estimated. Relative volumes of the apatite, the allanite, and the epidote zone were determined by point counting several BSE images, which gave a mean of 24 vol% apatite (including thorite inclusions), 33 vol% allanite, and 43 vol% epidote. These volumes correspond to 21 wt% apatite, 38 wt% allanite, and 41 wt% epidote, using average densities of 3.3 g/cm^3 (apatite), 4.2 g/cm^3 (allanite), and 3.5 g/cm^3 (epidote).

Using these weight proportions and the chemical data

TABLE 3. Average analyses of monazite cores, rims, and the mineral zones from the alteration corona

	Mnz core (n = 22)	Mnz rim (n = 18)	Ap zone (n = 12)*	Aln zone (n = 13)	Ep zone (n = 14)
P_2O_5	27.99 ± 0.75	28.45 ± 0.75	37.03 ± 2.90	—	—
SiO_2	0.50 ± 0.30	0.43 ± 0.20	2.10 ± 1.49	32.39 ± 0.51	35.76 ± 0.62
La_2O_3	13.24 ± 0.94	12.66 ± 1.08	0.67 ± 0.57	5.63 ± 0.50	2.39 ± 0.19
Ce_2O_3	27.36 ± 1.06	26.70 ± 1.51	1.25 ± 0.96	11.30 ± 0.91	5.72 ± 0.40
Pr_2O_3	3.66 ± 0.30	3.67 ± 0.13	0.20 ± 0.20	1.58 ± 0.13	0.84 ± 0.20
Nd_2O_3	12.00 ± 0.63	11.93 ± 0.50	0.48 ± 0.43	4.33 ± 0.29	2.96 ± 0.21
Sm_2O_3	2.11 ± 0.28	2.42 ± 0.39	0.11 ± 0.07	0.77 ± 0.19	0.85 ± 0.31
Y_2O_3	1.49 ± 0.51	2.24 ± 0.47	0.19 ± 0.06	0.42 ± 0.14	1.19 ± 0.25
ThO_2	8.23 ± 1.37	7.85 ± 1.50	5.69 ± 2.86	1.48 ± 0.20	0.39 ± 0.13
UO_2	0.27 ± 0.13	0.42 ± 0.25	0.18 ± 0.15	0.05 ± 0.03	0.23 ± 0.09
Al_2O_3	—	—	—	18.22 ± 0.99	23.01 ± 1.28
FeO	—	—	—	10.36 ± 0.79	7.90 ± 0.53
CaO	1.40 ± 0.28	1.44 ± 0.17	49.96 ± 3.71	11.29 ± 1.02	15.68 ± 0.98
MgO	—	—	—	0.42 ± 0.04	0.40 ± 0.05
Total	98.25	98.20	97.86	98.23	97.33

* Composition of the apatite zone is an average of 12 integrated analyses from four grains using a beam diameter of 5 μm. See text for further details.

given in Table 3, the mean chemical composition of the corona was calculated, i.e., the chemical composition of a mixture zone. The result, given in column 1 of Table 4, shows that the non-monazite elements (SiO_2, Al_2O_3, FeO, CaO, and trace MgO) make up approximately 75 wt% of the corona. The remaining monazite elements, given in column 2 of Table 4 (La, Ce, Pr, Nd, Sm, Th, U, Y, P), have been normalized to a total of 97 wt% (column 3 of Table 4). This total is reasonable for these elements in monazite because small amounts of Si, Ca, Gd, and HREE are not considered in the calculation. The resulting normalized monazite composition is strikingly similar to that measured at the rims of the preserved monazites (compare columns 3 and 4 in Table 4). Uranium and Y contents are slightly higher and La and Ce contents are slightly lower in column 3 compared to column 4. Indeed, it appears reasonable to assume that the primary monazite rim, which had been replaced through reaction, was slightly higher in Y and U and lower in Ce and La than the present monazite rim, considering the zoning patterns recorded in the preserved monazites (Table 3). The approximately 25 wt% theoretical monazite in the corona system (column 2 of Table 4) matches well with the textural observation that the apatite zone is directly replacing a former monazite rim, since the apatite zone also makes up about 25 wt% of the corona system according to the results of point counting.

Although the calculations certainly suffer from some uncertainties inherent to the analytical and modal averages used, the modeling basically suggests closed system behavior for the elements released through monazite breakdown. However, although the overall budget appears well balanced, it should be kept in mind that the process of monazite destruction leads to significant *small-scale* elemental redistribution between the mineral zones, effectively concentrating U, Y, HREE, and MREE, relative to LREE toward the margin of the corona zone (Table 3).

This kind of internal element fractionation throughout the corona may have important consequences when rocks with altered monazite are exposed to penetrative leaching through fluids or to non-equilibrium partial melting processes. The enhanced mobilization of the U, Y, HREE, and MREE relative to the LREE could result if the outer zone is preferentially affected by such a process. Likewise, strong trace and REE fractionation is feasible in the possible case of selective instability of the allanite or apatite zones.

Nature of the monazite breakdown and reaction

Textures show unequivocally that monazite was not stable during amphibolite facies regional metamorphism of the granitoid rock studied here. However, as mentioned previously, not all monazite grains were subjected to alteration. Armoring of the monazite crystals by minerals with low intracrystalline diffusion coefficients prevented breakdown and corona development. This is well illustrated in Figure 2 (grain 3) where no reaction rim has developed in the place where the monazite crystal surface is shielded by an epitactic zircon. Several monazites were also observed that had survived intact as armored inclusions within apatite. Conversely, the breakdown of monazite was most pronounced in crystals located along grain boundaries or cleavage planes of major minerals. These observations suggest that the basic requirement for activating the breakdown process is the presence of a metamorphic fluid phase which delivered Ca, Fe, Si, and Al to monazite grain boundaries. However, considering the distinct concentric alteration textures, it appears that the actual reaction kinetics were controlled by element diffusion from the monazite into the corona minerals and vice versa. At the *P-T* conditions and time scale of the regional metamorphic event, elemental diffusivities were apparently too low for complete monazite consumption. Thus, the extent of corona development around monazite may serve as an indicator of the time that a granitoid rock spent at elevated metamorphic *P-T* conditions.

Microtextures suggest that the new apatite was able to

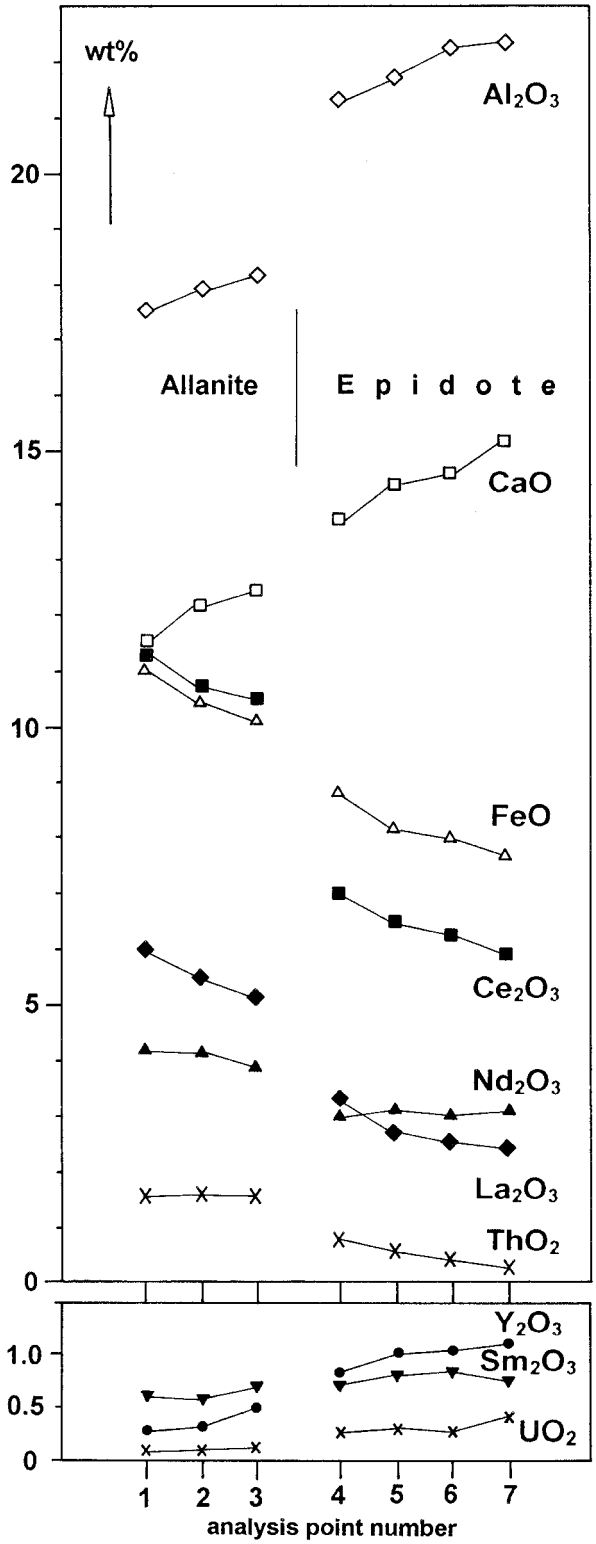

FIGURE 4. Zoning profile outward across the allanite and epidote zones of a representative grain. Note the two different Y-axis scales. The analysis points 1 to 7 are in a line and approximately 2 μm apart, except for points 3 and 4 (about 4 μm apart).

TABLE 4. Results of mass balance calculations

	1	2	3	4
P_2O_5	7.96	7.96	30.37	28.45
SiO_2	27.26	—	—	0.43
La_2O_3	3.24	3.24	12.37	12.66
Ce_2O_3	6.86	6.86	26.18	26.70
Pr_2O_3	0.98	0.98	3.74	3.67
Nd_2O_3	2.95	2.95	11.24	11.93
Sm_2O_3	0.66	0.66	2.51	2.42
Y_2O_3	0.68	0.68	2.61	2.24
ThO_2	1.94	1.94	7.40	7.85
UO_2	0.15	0.15	0.58	0.42
Al_2O_3	16.26	—	—	—
FeO	7.13	—	—	—
CaO	21.39	—	—	1.44
MgO	0.32	—	—	—
Total	97.78	25.43	97.00	98.20

Note: Column 1 shows the composition of an apatite-allanite-epidote mixture using the estimated modal proportions of each mineral in the corona and their average compositions from Table 3. Column 2 is the composition of the corona minus the "non-monazite" elements. As a simplification, Si and Ca have been treated as non-monazite elements, although small amounts are present. The values in Column 2 are then recast to 97 wt% in Column 3. Column 4 is the measured average composition of monazite rims from Table 3. Note that the close similarity between Columns 3 and 4 indicates closed-system behavior.

grow only within, or at least very close to, the former monazite lattice. Thus, it seems that the PO_4 tetrahedra of the monazite served directly as building blocks for the growth of apatite. Because the REE have particularly low diffusion coefficients in accessory minerals (Liang and Watson 1995), it may be assumed that the LREE released during monazite breakdown only diffused very slowly through the apatite zone outward into the allanite/epidote corona. In any case, the reaction rate would decrease as the apatite zone grew. This reduced reaction rate, coupled with insufficient time at elevated temperature, probably explains why complete destruction of the monazite cores was never attained.

Unlike the apatite front that advanced inward into the monazite, the allanite and the epidote ring formed as a fringe outside of the original monazite grain. Protrusions of allanite into the epidote zone suggest that allanite was successively replacing earlier-formed epidote. Likewise, the epidote ring enlarged outward, commonly invading the host minerals preferentially along their cleavages (Fig. 2, grain 3), which served either as channels for the metamorphic fluids or as energetically favorable sites for accessory mineral growth. The nucleation and growth of the high-LREE allanite ring adjacent to the apatite is governed most likely by the particularly high LREE concentration in this location. Decreasing availability of LREE away from the apatite probably resulted in the formation of the LREE-poorer epidote ring only. This interpretation is supported by the fact that both the allanite and the epidote zone have similar internal chemical gradients in which the LREE decrease outward (Fig. 4). It is interesting that discrete allanite and epidote growth rings formed during reaction, rather than one continuously zoned allanite-epidote solid solution. These rings may suggest a miscibility gap between these two phases. However, as

TABLE 5. Central European examples of amphibolite facies metagranitoids with Ap-Aln-Ep coronas around monazite

Rock	Protolith type	Locality
Alpeiner granodioritic gneiss	high-K I-type, medium-grained Bt-granodiorite	
Sulztal granite gneiss	Kfs phyric S-type Bt granite ±Crd	central Ötztal-Stubai crystalline basement (Austro-alpine unit)
Winnebach migmatite gneiss	granitic to granodioritic Crd-bearing S-type diatexite	
Granatspitz granite gneiss	medium to coarse-grained two-mica Crd-bearing S-type granite	central Tauern Window
Hochweissenfeld granite gneiss	Kfs phyric high-K I-type Bt granite	
Zinken granite gneiss	fine-grained leucocratic S-type two mica granite	Seckau-Bösenstein Massif (Austro-alpine unit)
Waldbach granite gneiss	fine- to medium-grained leucocratic S-type two mica granite	Raabalpen Massif (Austro-alpine unit)
Weitersfeld "pencil" gneiss	evolved I-type granite	Moravian Unit, eastern Bohemian Massif, Austria
Bittesch gneiss	evolved I-type granite	
Liesnica gneiss	migmatite	Veporic unit, Slovenske Rudohorie, Carpathian Mountains

Note: P-T estimates for all the rocks are in the range 500–600 °C and 4–7 kbar (Hoernes and Friedrichsen 1974; Frank et al. 1987; Bernroider 1989; Hoinkes and Thöni 1993; Plasienka et al. 1997; Schermaier et al. in press).

yet no experimental data are available on the solid solution relationship between epidote and allanite.

The bulk of Y released from the former monazite was apparently able to move across the allanite zone into the epidote zone where it concentrated mainly near the outer rim of the corona. It appears that Y was pushed successively rimward due to its poor fit in the allanite-epidote lattice sites, whereas the LREE were preferentially trapped in proximal sites. The HREE have probably behaved in a similar fashion to Y in view of their similar ionic radii. Figure 4 shows that the MREE, such as Sm, display behavior intermediate to Y and LREE. Uranium was redistributed similar to Y and was concentrated in the epidote zone, whereas Th became trapped mainly in the apatite zone as indicated by the presence of many tiny thorite inclusions. Despite such localized mobility, mass-balance calculations reveal that none of the former monazite constituents was able to leave the corona system in significant amounts. This finding supports the claim that elements such as U, Th, Y, and the REE are highly immobile during metamorphism.

Whether the observed breakdown of monazite can be described by a stoichiometric reaction is difficult to answer. It is likely that the Ca required to form apastite and epidote-allanite was provided by the breakdown of the anorthite component in plagioclase. The Fe needed for the formation of allanite-epidote could be derived from the metamorphic breakdown of biotite, and the potassium thus liberated may have been consumed in the formation of muscovite (together with Al remaining from the anorthite breakdown). However, in view of the low reaction rate and the few external atoms required, the necessary amounts of Ca, Fe, Si, and Al could be supplied simply by a fluid phase chemically buffered through other metamorphic reactions and by the solubility equilibria of the major mineral components of the rock.

Stability of monazite during regional metamorphism

The textures noted here do not appear to have been previously described in the literature. However, the replacement of primary monazite by apatite-allanite-epidote coronas is common in many S-type and high-K I-type amphibolite facies metagranitoids from the Alps, Carpathians and eastern Bohemian massif (Table 5). Thus, monazite seems to be unstable under normal amphibolite facies conditions in granitoid lithologies. Previous work shows that, where newly formed monazite crystals were found in metagranitoid rocks, metamorphic temperatures were always in excess of 700 °C (e.g., Schenk and Todt 1983; Friedl et al. 1994; Bingen et al. 1996; Büttner and Kruhl 1997).

In contrast, it is well known that amphibolite facies metapelites commonly contain newly formed metamorphic monazite, as demonstrated in many geochronological studies worldwide (e.g., Parrish 1990 and references therein). Smith and Barreiro (1990) document a case where monazites grew in pelitic shists under prograde conditions near the staurolite-in isograd at conditions as low as ca. 525 °C and 3 kbar. Franz et al. (1996) report metamorphic monazite growth between 450 and 700 °C in low pressure–high temperature metapelites in northern Bavaria. A particularly convincing situation occurs in the Moravian Unit in the eastern part of the Bohemian Massif. Here, at metamorphic conditions of 500–550 °C and 4–5 kbar (Bernroider 1989), new monazites grew in metapelitic paragneisses, whereas interlayed granitic orthogneisses contain primary monazite with Ap-Aln-Ep coronas (Finger et al. 1996 and unpublished data).

Implications for U-Th-Pb monazite geochronology

Monazite has been shown to be useful for dating magmatic and high-temperature metamorphic events (Parrish 1990). This usefulness results from the fact that monazite

FIGURE 5. Sketch showing grain 7 (Fig. 2) with the results of U-Th-Pb chemical dating (in Ma) included in the circles. Data also given in Table 5.

TABLE 6. Results of U-Th-Pb chemical model age dating grain 7*

Analysis	Th	U	Pb	Age
m 7–6	8.184	0.375	0.132	314 ± 43
m 7–7	7.066	0.306	0.119	330 ± 50
m 7–8	8.279	0.349	0.141	335 ± 43
m 7–9	7.535	0.472	0.132	327 ± 45
m 7–10	7.180	0.405	0.132	347 ± 49
m 7–11	7.810	0.336	0.135	339 ± 45
m 7–13	6.588	0.465	0.116	321 ± 50
weighted average				330 ± 10
apatite 1	6.653	0.358	0.009	27 ± 53
apatite 2	2.731	0.158	0.008	56 ± 125
apatite 3	5.607	0.275	0.005	17 ± 63

* See Figures 2 and 5. Model ages calculated using the method of Montel et al. (1996) given here in the appendix. Also included are three analyses from the apatite zone of another grain.

is highly retentive (i.e., it frequently exhibits closed-system behavior) and it has a high-closure temperature of roughly 725 °C. The typically high concentrations of U and Th in monazite also contribute to the reliability of the age dates. As a result, monazite very often provides highly precise and concordant U-Th-Pb ages.

In the case of amphibolite facies metamorphic rocks, most published concordant monazite ages have been obtained from paragneisses, where monazite formed during regional metamorphism. A few studies have attempted to date primary monazite relics from orthogneisses using U-Pb isotope systematics. In these cases, strongly discordant results were obtained from multi-grain monazite fractions, which yielded Pb-Pb ages older than the metamorphic event (Mougeot et al. 1997; Friedl 1997). Based on the observations made in the present study, discordant results may be attributed to one or both of the following: (1) The monazites themselves suffered little or no Pb loss, but the analyzed fractions contained monazite with secondary coronas that contained a metamorphic U-Pb component. (2) The monazites themselves lost radiogenic Pb during metamorphism, e.g., through diffusion around misoriented domains on the sub-micrometer scale (Black et al. 1984), but were not completely reset.

For the Granatspitz granite gneiss, it was instructive to test to what extent the monazite cores of the pseudomorphs have preserved their primary lead contents. To do this, high-precision electron microprobe measurements were carried out for Th, U, and Pb in one of the monazite grains (Fig. 5), using high beam currents and long counting times (for analytical procedure see appendix). The resultant data permit calculation of the total Pb monazite model ages (Suzuki et al. 1991; Montel et al. 1996), assuming that the measured Pb is entirely radiogenic. This assumption is reasonable, as common Pb is generally less than 1% of the total Pb in monazites having Paleozoic and older ages (e.g., Parrish 1990).

The results of the analyses, given in Table 6, suggest that the preserved monazite cores did not experience major Pb loss during Alpine metamorphism. Pb contents in seven analysis points of the measured monazite grain yield Variscan model ages (Fig. 5). The weighted average age calculated for these analyses is 330 Ma, which is in perfect agreement with previous 320–330 Ma zircon and Rb-Sr whole-rock ages (Cliff 1981). Of course, because the precision of the microprobe dating technique is limited, slight Pb loss, corresponding to a few million years time, could remain undetected.

U-Th-Pb analyses were also carried out in the apatite zone of another grain, which was wide enough to allow analysis with a 5 μm diameter beam. Here hardly any Pb was detected, despite the high Th contents due to the thorite intergrowths in some cases (Table 6). These low Pb contents are compatible with the much younger metamorphic age obtained from the apatite zones.

Thus U-Th-Pb microprobe data suggest that the metastable monazites from amphibolite facies orthogneisses may well be suitable for revealing magmatic protolith ages, particularly where ion microprobe or laser ablation ICP-MS can be applied. Strong discordancies of multi-grain monazite fractions, combined with enhanced common Pb contents as shown by Mougeot et al. (1997) and Friedl (1997), may be dominantly due to the presence of secondary alteration rims. When using conventional U-Pb multi-grain analysis, it is crucial that metamorphic coronas be removed through abrasion, if possible, together with potential thin marginal lead loss zones of the monazite itself. We expect that such drastically abraded fractions will provide near concordant ages in many cases.

As previously mentioned, several monazites remained unaffected by the transformation process, because they were protected as inclusions in magmatic apatites. For dating purposes, such crystals could be particularly useful. These may be recognized in heavy mineral grain mounts by their euhedral shape and high transparency. Conversely corona-bearing monazites always appeared as dull, rounded grains.

ACKNOWLEDGMENTS

This paper resulted mainly from research work carried out in the frame of a Lise Meitner fellowship project (M00150-GEO) to Broska. The Austrian FWF is thanked for financial support. Parts of the fieldwork were kindly supported by the BMWF through grant OWP 39. Hans Steyrer is gratefully thanked for his invaluable drafting of some of the figures. David

Wark and Antonio Lanzirotti provided us with thought-provoking reviews that improved the clarity and significance of this work. Last, but by no means least, we would like to express our thanks to Volker Höck for his successful efforts in obtaining the microprobe facility at Salzburg University.

REFERENCES CITED

Bea, F. (1996) Residence of REE, Y, Th and U in granites and crustal protoliths; Implications for the chemistry of crustal melts. Journal of Petrology, 37, 521–552.

Benisek, A. and Finger, F. (1993) Factors controlling the development of prism faces in granite zircons: A microprobe study. Contributions to Mineralogy and Petrology, 114, 441–451.

Bernroider, M. (1989) Zur Petrogenese präkambrischer Metasedimente und cadomischer magmatite im Moravikum. Jahrbuch der Geologische Bundesanstalt, 132, 349–373.

Bingen, B., Demaiffe, D., and Hertogen, J. (1996) Redistribution of rare earth elements, thorium, and uranium over accessory minerals in the course of amphibolite to granulite metamorphism: The role of apatite and monazite in orthogneisses from southwestern Norway. Geochimica et Cosmochimica Acta, 60, 1341–1354.

Black, L.P., Fitzgerald, J.D., and Harley, S.L. (1984) Pb isotopic composition, colour, and microstructure of monazites from a polymetamorphic rock in Antarctica. Contributions to Mineralogy and Petrology, 85, 141–148.

Bons, A.J. (1988) Intracrystalline deformation and slaty cleavage development in very low-grade slates from the central Pyrenees. Geologica Ultraiectina, 56.

Büttner, S.H. and Kruhl, J. (1997) The evolution of a late Variscan high-T/low-P region: The south-eastern margin of the Bohemian massif. Geologische Rundschau, 86, 21–38.

Cliff, R.A. (1981) Pre-Alpine history of the Pennine zone in the Tauern Window, Austria: U-Pb and Rb-Sr geochronology. Contribution for Mineralogy and Petrology, 77, 262–266.

Cocherie, A. (1984) Interaction manteau-croûte: son rûle dans la genèse d'associations plutoniques calco-alcalines, contraintes géochimiques (élements en traces et isotopes du strontium et de l'oxygène), 246 p. Ph.D. thesis, Université de Rennes, Rennes.

Dachs, E. (1986) High-pressure mineral assemblages and their breakdown-products in metasediments south of the Grossvenediger, Tauern window, Austria. Schweizer Mineralogisch Petrographische Mitteilungen, 66, 145–161.

Dollase, W.A. (1971) Refinement of the crystal structures of epidote, allanite and hancockite. American Mineralogist, 56, 447–464.

Exley, R.A. (1980) Microprobe studies of REE-rich accessory minerals: Implications for Skye granite petrogenesis and REE mobility in hydrothermal systems. Earth and Planetary Science Letters, 48, 97–110.

Finger, F., Frasl, G., Haunschmid, B., Lettner, H., Schermaier, A., Schindlmayr, A.O., Steyrer, H.P., and von Quadt, A. (1993) The zentralgneise of the Tauern Window (Eastern Alps): Insight into an Intra-Alpine Variscan batholith. In F. Neubauer and J. von Raumer, Eds., The pre-Mesozoic Geology in the Alps, p. 375–391. Springer Verlag, Berlin.

Finger, F., Benisek, A., Broska, I., Friedl, G., Haunschmid, B., Schermaier, A., Schindlmayer, A., Schitter, F., and Steyrer, H.P. (1996) Altersdatieren von Monaziten mit der Elektronenmikrosonde-eine wichtige neue Methode in den Geowissenschaften, p. 118–122. 6th Symposium Tektonik-Strukturgeologie-Kristallingeologie, Universität Salzburg, Abstracts.

Frank, W., Höck, V., and Miller, C. (1987) Metamorphic and tectonic history of the Central Tauern Window. In H.W. Flügel and P. Faupl, Eds., Geodynamics of the Eastern Alps, p. 34–55. Deuticke, Wien.

Franz, G., Andrehs, G., and Rhede, D. (1996) Crystal chemistry of monazite and xenotime from Saxothuringian-Moldanubian metapelites, NE Bavaria, Germany. European Journal of Mineralogy, 8, 1097–1118.

Frasl, G. (1958) Zur Seriengliederung der Schieferhülle in den Mittleren Hohen Tauern. Jahrbuch der Geologische Bundesanstalt, 101, 323–472.

——— (1967) Glimmerpseudomorphosen nach Cordierit im Zentralgneis des Granatspitzkerns, Hohe Tauern. Mineralogische Mitteilungen Joanneum, 1(2), 11–17.

Friedl, G. (1997) U/Pb Datierungen an Zirkonen und Monaziten aus Gesteinen vom österreichischen Anteil der Böhmischen Masse, 242 p. Ph.D. thesis, Universität Salzburg, Salzburg.

Friedl, G., von Quadt, A., and Finger, F. (1994) 340 Ma U/Pb-Monazitalter aus dem niederösterreichischen Moldanubikum und ihre geologische Bedeutung. Terra Nostra, 3(94), 43–46.

Hoernes, S. and Friedrichsen, H. (1974) Oxygen isotope studies on metamorphic rocks of the Western Hohe Tauern area (Austria). Schweizer Mineralogische und Petrographische Mitteilungen, 51, 769–788.

Hoinkes, G. and Thöni, M. (1993) Evolution of the Ötztal-Stubai, Scarl-Campo and Ulten Basement Units. In F. Neubauer and J. von Raumer, Eds., The pre-Mesozoic Geology in the Alps, p. 485–494. Springer Verlag, Berlin.

Kretz, R. (1983) Symbols for rock-forming minerals. American Mineralogist, 68, 277–279.

Lanzirotti, A. and Hanson, G.N. (1996) Geochronology and geochemistry of multiple generations of monazite from the Wepawaug Schist, Connecticut, USA: Implications for monazite stability in metamorphic rocks. Contributions to Mineralogy and Petrology, 125, 332–340.

Liang, Y. and Watson, E.B. (1995) A simple model for sector zoning in slowly grown crystals: Implications for growth rate and lattice diffusion, with emphasis on accessory minerals in crustal rocks. American Mineralogist, 80, 1179–1187.

Montel, J.M. (1993) A model for monazite/melt equilibrium and application to the generation of granitic magmas. Chemical Geology, 110, 127–146.

Montel, J.M., Foret, S., Veschambre, M., Nicollet, C., and Provost, A. (1996) Electron microprobe dating of monazite. Chemical Geology, 131, 37–53.

Mougeot, R., Respaut, J.P., Ledru, P., and Marignac, C. (1997) U-Pb geochronology on accessory minerals of the southern edge of the Velay granite (French Massif Central). European Journal of Mineralogy, 1, 141–156.

Overstreet, W.C. (1967) The geological occurence of monazite. U.S. Geological Survey Professional Paper, 530.

Parrish, R.R. (1990) U-Pb dating of monazite and its application to geological problems. Canadian Journal of Earth Sciences, 27, 1431–1450.

Petrik, I., Broska, I., Lipka, J., and Siman, P. (1995) Granitoid allanite-(Ce): Substitution relations, redox conditions and REE distributions (on an example of I-type granitoids, Western Carpathians, Slovakia). Geologica Carpathica, 46, 79–94.

Plasienka, D., Janak, M., Frey, M., and Schmidt, S.T. (1997) Structural and metamorphic evolution of a cretaceous core complex: The Veporic superunit of the central Western Carpathians (Slovakia). Terra Nova, 9, Abstract Supplement, 1, 158.

Rapp, R.P. and Watson, E.B. (1986) Monazite solubility and dissolution kinetics: Implications for thorium and light rare earth element chemistry of felsic magmas. Contributions to Mineralogy and Petrology, 94, 304–316.

Sawka, W.N. (1988) REE and trace element variations in the accessory minerals and hornblende from the strongly zoned McMurray Meadows Pluton, California. Transactions of the Royal Society of Edinburgh, 79, 157–168.

Schenk, V. and Todt, W. (1983) U-Pb-datierungen an Zirkon und Monazit der Granulite im Moldanubikum Niederösterreichs (Waldviertel). Fortschritte der Mineralogie, 61, 190–191.

Schermaier, A., Haunschmid, B., and Finger, F. (1997) Distribution of Variscan I- and S-type granites in the Eastern Alps: A possible clue to unravel pre-Alpine basement structures. Tectonophysics, 272, 315–333.

Schitter, F. (1997) Spurenelementkonzentration in den gesteinsbildenden Mineralien des Gebhartser Diorits und des Eisgarner Granits, bestimmt mittels der Instrumentellen Neutronenaktivierungsanalyse, 75 p. Diplomarbeit thesis, Universität Salzburg, Salzburg.

Smith, H.A. and Barreiro, B. (1990) Monazite U-Pb dating of staurolite grade metamorphism in pelitic schists. Contributions to Mineralogy and Petrology, 105, 602–615.

Steiger, R.H. and Jäger, E. (1977) Subcommission on geochronology: Convention on the use of decay constants in geo- and cosmochronology. Earth and Planetary Science Letters, 36, 359–362.

Suzuki, K., Adachi, M., and Tanaka, T. (1991) Middle Precambrian provenence of Jurassic sandstones in the Miro Terrane, central Japan: Th-

U-total Pb evidence from an electron microprobe monazite study. Sedimentary Geology, 75, 141–147.
von Quadt, A. and Finger, F. (1991) Geochronologische Untersuchungen im österreichischen Teil des Südböhmischen Batholiths: U-Pb Datierungen an Zirkonen, Monaziten und Xenotimen des Weinsberger Granits. European Journal of Mineralogy, 3, Beiheft 1, 281.
Wakita, H., Rey, P., and Schmitt, R.A. (1971) Abundances of 14 rare-earth elements and 12 other trace elements in Apollo 12 samples: five igneous and one breccia rocks and four soils. Proceedings of the 2nd Lunar Science Conference, 1319–1329.
Ward, C.D., McArthur, J.M., and Walsh, J.N. (1991) Rare earth element behaviour during evolution and alteration of the Dartmoor granite, SW England. Journal of Petrology, 33, 785–815.
Wark, D.A. and Miller, C.F. (1993) Accessory mineral behaviour during differentiation of a granite suite: Monazite, xenotime and zircon in the Sweetwater Wash pluton, southeastern California, USA. Chemical Geology, 110, 49–67.

Manuscript received February 19, 1997
Manuscript accepted November 1, 1997

Appendix: Electron microprobe analytical techniques and chemical model-age calculations

Measurements were carried out on a Jeol JX 8600 instrument equipped with three wavelength-dispersive spectrometers. Except for the determination of chemical monazite ages (see below), operating conditions were 15 kV and 30 nA, usually with a maximally focused beam of about 1 μm diameter. All elements were counted for 10 s at the peak and for 2 × 3 s at the background positions. Under these conditions, detection limits of about 0.03–0.1 wt% could be obtained. ZAF corrections were routinely applied. X-ray lines were chosen according to the suggestions of Exley (1980). Commercially available synthetic glass standards were used for the REE. Standards used for the other trace elements are discussed by Benisek and Finger (1993).

Electron microprobe analysis of very narrow mineral zones in the coronas is particularly problematic, because X-rays may excite not only elements from the phase of interest, but also those of adjacent minerals that fall within the excitation volume of the electron beam. This can potentially lead to analyses that represent mixtures of two phases, rather than just that of the desired phase. To minimize this risk, the analysis points were set at least 2 μm away from the margins of the phases. Analyses were considered valid only when their stoichiometry was ''perfect.'' Analyses of apatite obtained 2 μm away from the contact with allanite lack any Fe and Al, which indicates that any external compositional influence is mostly negligible over this distance.

For the determination of total lead monazite model ages, which require a particularly precise measurement of Pb in the 0.1–0.2 wt% range, the probe current was increased to 250 nA at 15 kV. The beam size was enlarged to 5–10 μm diameter to avoid damage to the sample. For the analysis of Pb, counting times were 100 s (peak) and 2 × 50 s (background). Counting times for the Th and U were also extended to 30 s (2 × 15 s) and 50 s (2 × 25 s), respectively. Additionally, the elements La, Ce, Pr, Nd, Sm, P, and Y were determined with 10 s (2 × 3 s) counting times to enable a reasonable ZAF correction. A small Y interference on the Pb$M\alpha$ line was eliminated by measuring a Pb-free yttrium standard and routinely correcting the monazite analyses by linear extrapolation (Montel et al. 1996).

For every measured point, the model age (τ) was calculated by solving the following equation (see Montel et al. 1996):

$$\mathrm{Pb} = \mathrm{Th}/232[\exp(\lambda^{232}\tau) - 1]208 + (\mathrm{U}/238.04)0.9928 \times [\exp(\lambda^{238}\tau) - 1]206 + (\mathrm{U}/238.04)0.0072 \times [\exp(\lambda^{235}\tau) - 1]207$$

where U, Th, and Pb concentrations are in parts per million, and λ^{232}, λ^{238}, and λ^{235} are the radioactive decay constants of ^{232}Th, ^{238}U, and ^{235}U, respectively (Steiger and Jäger 1977). The 2σ errors for the single model ages were calculated by propagating the Th, U, and Pb errors as resulting from the counting statistics of the microprobe (Montel et al. 1996). These were typically ± 0.04–0.05 wt% for the Th, ± 0.025–0.030 wt% for the U, and ± 0.018–0.020 wt% for the Pb, at 250 nA, 15 kV (all 2σ errors). To control the quality of the analyses, monazites with precisely known concordant U-Pb ages were measured together with the unknown sample. A weighted average of 324 ± 18 Ma was obtained from the standard monazites, which is in perfect agreement with the conventional U-Pb age of 318 ± 4 Ma (von Quadt and Finger 1991).